On the Applicability of the Surface Impedance Integral Equation for Optical and Near Infrared Copper Dipole Antennas

George W. Hanson, *Senior Member, IEEE*

***Abstract*—The applicability of the surface impedance integral equation (SI-IE) method for the analysis of optical and near-infrared copper dipole antennas is assessed, and some issues relative to resonant half-wavelength optical dipoles are highlighted. Since at these frequencies the conductivity of copper (and of all metals) is relatively small, the appropriateness of using the standard integral equation method for imperfectly conducting wires, based on a surface impedance boundary condition, needs to be examined. Here it is found that the SI-IE method yields accurate results in the near-infrared regime, and for suitably small wire radius values at low optical frequencies. For the middle and upper optical frequencies the approximate SI-IE is not generally valid. Some results are presented for a half-wave dipole resonant in the upper near-infrared/low optical range, and a discussion of the trade-off between maintaining good polarization selectivity and radiation efficiency is provided.**

***Index Terms*—Cylindrical antennas, electromagnetic theory, nanotechnology, optical antenna.**

I. Introduction

OPTICAL antennas are of interest due to the promise of having a very small (wavelength or even subwavelength) optical receiving and transmitting element that exhibits good polarization and frequency selectivity. Recent advances in fabrication technologies have made possible the production of metallic cylindrical rods having radius values well under 100 nm, with well-controlled lengths [1], [2]. Thus, it is now possible to make nanostructures with sufficient precision to fabricate nanoantennas, and there is interest in applying antenna techniques that are common in, say, the megahertz and gigahertz range, to the upper terahertz and optical ranges [3]–[7].

The purpose of this work is twofold. The first aim is to assess the applicability of standard surface-impedance integral equation methods for the analysis of optical (380–750 THz) and near infrared (60–380 THz) copper dipole antennas. At optical frequencies and in the near infrared the conductivity of copper is not large, and the appropriateness of using the standard (for megahertz and gigahertz technologies) integral equation method for imperfectly conducting wires, based on a surface impedance boundary condition, needs to be considered. The second aim is to provide a brief discussion of the feasibility of obtaining an optical dipole antenna which would resemble, physically and electrically, a miniaturized version of the classic half-wave resonant dipole antenna that is the workhouse of the wireless industry. One can consider the classic dipole antenna to have a large length-to-radius ratio, and an electrically small radius, leading to excellent polarization selectivity and desirable radiation patterns. Scaling down to the nanoscale, it is concluded here that one can achieve a moderately large length-to-radius ratio in the near-infrared band, and at the lowest optical frequencies. However, in the middle to upper optical range, the extremely small resonant length, generally well less than 200 nm, and the finite value of copper's conductivity (which places limits on the wire radius if one is to maintain a reasonable level of antenna efficiency), leads to the conclusion that, at best, relatively small length-to-radius values (on the order of 5–10) can be obtained, which will impact the polarization selectivity and radiation pattern of the dipole.

As far as the modeling of the antenna is concerned, it is clear that the perfectly conducting wire model will not work at optical frequencies and in the near-infrared, due to the relatively low optical conductivity of metals. That leaves several choices for constructing an integral equation model. One could use the imperfect conductor model, where the conductivity is sufficiently high such that one can define a surface impedance boundary condition. This method leads to an approximate integral equation, which we call the surface-impedance integral equation (SI-IE) that works extremely well for the noble metals [copper (Cu), gold (Au), and silver (Ag)], and other good conductors at megahertz, gigahertz, and lower terahertz frequencies [8]–[12]. Next to the perfect conductivity model, this surface impedance formulation is the simplest. Otherwise, one has to treat the material as a lossy dielectric, and use either volume integral equations, or the surface equivalence principle to form surface integral equations. Both methods can be used to lead to exact formulations, although the computational complexity grows rapidly for these methods, compared to computational methods for the perfect-conductivity model and the surface impedance formulation. Of the two exact formulations, volume integral equations have the advantage that extremely inhomogeneous, anisotropic materials can be easily modeled (since it is a direct-space discretization), at the expense of relatively high computational cost. In the literature, optical nanostructures, some of which resemble antenna-like finite length wires, have been modeled using predominately volume integral equations [13]–[16]. Although these papers address several wire-like structures, they are not focused specifically on antennas. However, optical dipoles have been modeled using the coupled dipole formulation [17], and optical bowties have been analyzed by the finite-difference time-domain (FDTD) method [18], [19]. In the far infrared regime, surface impedance integral

Manuscript received November 7, 2005; revised June 22, 2006.

The author is with the Department of Electrical Engineering, University of Wisconsin-Milwaukee, Milwaukee, WI 53211 USA (e-mail: george@uwm.edu).

Digital Object Identifier 10.1109/TAP.2006.886516

equations have been used to model printed dipoles [20]. Experimental results for pulsed optical bowties [21] and for pulsed optical strip dipoles [22] have been presented. However, there is a relative paucity of experimental and theoretical/numerical work on optical and near-infrared dipoles and related structures.

In this paper, the approximate integral equation arising from the surface impedance boundary condition is discussed for optical and near-infrared dipoles, where it is shown to be a suitable model for copper dipoles in the near-infrared band and lower optical frequencies. We reach this conclusion by considering the special case of an infinite-length dipole constructed from a lossy dielectric, which can be analyzed exactly using model expansions and Fourier transforms. This exact solution can be compared to the *exact* solution of the *approximate* SI-IE for the infinite-length dipole. As a further check on these results, another comparison is made to the *approximate* solution [based on the method of moments (MoM)] of the SI-IE for a long, yet finite-length dipole.

Having established the range of validity for the surface impedance integral equation, some results are then presented for the input impedance and efficiency of a half-wave dipole that is resonant in the upper near-infrared/low optical range, and the concept of an optical dipole is discussed.

II. Formulation

Consider first an infinite dielectric cylinder with axis coincident with the z-axis, having radius a and residing in free space. Let the cylinder have material parameters ε_m, μ_0, where ε_m is the complex permittivity. For this geometry two methods will be considered, an exact modal expansion and an approximate SI-IE that admits an exact solution.

A. Infinite Lossy Dielectric Cylinder—Exact Modal Expansion Solution

Working in the axial Fourier transform domain and assuming an azimuthally-independent magnetic ring (frill) current source having radius b, the incident fields can be written as [23, p. 373]

$$\left\{ \begin{array}{c} E_z^i(\rho,z) \\ H_\phi^i(\rho,z) \end{array} \right\} = \frac{b}{4} \int_{-\infty}^{\infty} \left\{ \begin{array}{c} j\kappa_0 J_0(\kappa_0\rho) \\ -\omega\varepsilon_0 J_1(\kappa_0\rho) \end{array} \right\} H_1^{(2)}(\kappa_0 b) e^{-j\alpha z} d\alpha \tag{1}$$

(an E_ρ component also exists, but is not needed here), where J_0 and J_1 are the zeroth- and first-order Bessel functions of the first kind, respectively, and $H_1^{(2)}$ is the first-order Hankel function of the second kind. The fields inside and outside the cylinder can be written as

$$E_z(\rho,z) = \int_{-\infty}^{\infty} \left\{ \begin{array}{c} a_0 J_0(\kappa_m\rho) \\ b_0 H_0^{(2)}(\kappa_0\rho) \end{array} \right\} e^{-j\alpha z} d\alpha \tag{2}$$

$$H_\phi(\rho,z) = \left\{ \begin{array}{cc} \frac{j\omega\varepsilon_m}{\kappa_m} & \frac{j\omega\varepsilon_0}{\kappa_0} \end{array} \right\} \int_{-\infty}^{\infty} \left\{ \begin{array}{c} a_0 J_1(\kappa_m\rho) \\ b_0 H_1^{(2)}(\kappa_0\rho) \end{array} \right\} e^{-j\alpha z} d\alpha \tag{3}$$

where the upper expressions are for $\rho \le a$ and the lower expressions are for $\rho \ge a$, and where $\kappa_m^2 = k_m^2 - \alpha^2, \kappa_0^2 = k_0^2 - \alpha^2, k_m^2 = \omega^2\mu_0\varepsilon_m$, and $k_0^2 = \omega^2\mu_0\varepsilon_0$. The unknowns a_0 and b_0 are determined by enforcing continuity of the tangential field components at the surface of the cylinder, $\rho = a$, leading to

$$a_0 = \frac{\varepsilon_0\kappa_m b}{2\pi a} \frac{H_1^{(2)}(\kappa_0 b)}{Z^e(\alpha)} \tag{4}$$

where

$$Z^e(\alpha) = \varepsilon_m\kappa_0 J_1(\kappa_m a) H_0^{(2)}(\kappa_0 a) - \varepsilon_0\kappa_m J_0(\kappa_m a) H_1^{(2)}(\kappa_0 a). \tag{5}$$

The zeros of $Z^e(\alpha)$ represent the symmetric TM modes of the dielectric cylinder.

The current density inside the cylinder, parallel to the cylinder axis, is

$$\begin{aligned} J_z(\rho,z) &= j\omega\varepsilon_m E_z(\rho,z) \\ &= j\omega\varepsilon_m \int_{-\infty}^{\infty} a_0 J_0(\kappa_m\rho) e^{-j\alpha z} d\alpha \end{aligned} \tag{6}$$

such that the cylinder current can be written as

$$\begin{aligned} I(z) &= \int_0^a \int_0^{2\pi} J_z(\rho,z)\rho d\phi d\rho \\ &= j\omega\varepsilon_m 2\pi a \int_{-\infty}^{\infty} \frac{a_0}{\kappa_m} J_1(\kappa_m a) e^{-j\alpha z} d\alpha. \end{aligned} \tag{7}$$

Therefore

$$\begin{aligned} I(z) &= I^e(z) \\ &= j\omega\varepsilon_m\varepsilon_0 b \int_{-\infty}^{\infty} \frac{J_1(\kappa_m a) H_1^{(2)}(\kappa_0 b)}{Z^e(\alpha)} e^{-j\alpha z} d\alpha. \end{aligned} \tag{8}$$

This is an exact solution, and so we denote the current by $I^e(z)$.

The factor $Z^e(\alpha)$ is multivalued in the α-plane due to the Hankel functions, and branch points appear at $\alpha = \pm k_0$. Branch cuts are chosen along the real-α axis, and exist along $-\infty < \alpha \le -k_0$, and $k_0 \le \alpha < \infty$. The path of integration in (8) is parallel to, and just below, the real axis for $-\infty < \alpha \le 0$, and parallel to, and just above, the real axis for $0 \le \alpha < \infty$. Following the method detailed in [24, pp. 451–453], (see also [23, pp. 377–380]) the integral (8) can be written as a branch cut integral and a sum of residues

$$I^e(z) = \sum_n I_n^e(z) + I_{\rm bc}^e(z) \tag{9}$$

where

$$I_n^e(z) = -2\pi j R_n^e(z) \tag{10}$$

with R_n^e denoting the residue associated with the nth zero of (5), i.e., values of α such that $Z^e(\alpha_n) = 0$. The branch cut integral has much better convergence properties than the original

integral (8), and is used for computing results in this work. The final form for the branch cut integral is

$$I^e_{\rm bc}(z) = k_0\omega\varepsilon_m\varepsilon_0 b\int_0^\infty \frac{ue^{-k_0z\sqrt{u^2-1}}}{\sqrt{u^2-1}} \times\left[F^{(1)}(u)-F^{(2)}(u)\right]du \tag{11}$$

where $F^{(n)}$ is given in (12), shown at the bottom of the page, and $\xi_m=\sqrt{k_m^2+k_0^2(u^2-1)}$.

B. Infinite Lossy Dielectric Cylinder—Approximate Surface Impedance Integral Equation

Because the modal method can not be used for finite length wires, the SI-IE for an infinite or finite length metal cylinder is now formed. If the conductivity of the cylinder is sufficiently large such that the surface impedance boundary condition is valid, and if circumferential currents and the azimuthal dependence of axial currents can be ignored (either due to the wire being electrically thin, or due to the specific excitation), the approximate current $I^a(z)$ satisfies the impedance boundary condition

$$I^a(z)Z_s = E_s(z) \tag{13}$$

at $\rho=a$, where Z_s is the surface impedance [see the Appendix for a derivation and discussion of (14)]

$$Z_s=\frac{\gamma J_0(\gamma a)}{2\pi a\sigma J_1(\gamma a)} \tag{14}$$

σ is the conductivity of the metal (S/m), and

$$\gamma=(1-j)\sqrt{\frac{\omega\mu_0\sigma}{2}}. \tag{15}$$

Expressing the electric field as the sum of an impressed field, E^i_z, and the field due to the resulting current leads to the standard Pocklington equation for the thin wire [9], [25]–[30]

$$\left(k_0^2+\frac{\partial^2}{\partial z^2}\right)\int_{-\infty}^{\infty}K\left(z-z'\right)I^a(z')dz' = j4\pi\omega\varepsilon_0\left(Z_sI^a(z)-E^i_z(z)\right) \tag{16}$$

where $K(z-z')$ is the kernel

$$K(z-z')=\frac{1}{2\pi}\int_{-\pi}^{\pi}\frac{e^{-jk_0\sqrt{(z-z')^2+4a^2\sin^2(\phi'/2)}}}{\sqrt{(z-z')^2+4a^2\sin^2(\phi'/2)}}d\phi'. \tag{17}$$

We next discuss the exact solution of (16), followed by the approximate solution of (16) when it is modified to pertain to the finite-length dipole.

1) Exact Solution of the Surface Impedance Integral Equation: Using Fourier transform methods ([23, pp. 290–292], [24, pp. 448–450]), we can solve (16) as

$$I^a(z)=4\omega\varepsilon_0\int_{-\infty}^{\infty}\frac{E^i_z(\alpha)e^{-j\alpha z}}{Z^a(\alpha)}d\alpha \tag{18}$$

where the path of integration is the same as for (8), and where

$$Z^a(\alpha)=\left(\kappa_0^2-\alpha^2\right)J_0(\kappa_0a)H_0^{(2)}(\kappa_0a)+4\omega\varepsilon_0Z_s. \tag{19}$$

Note that (18) is an *exact solution* to the *approximate* SI-IE (16). For the magnetic frill source

$$I^a(z)=j\omega\varepsilon_0 b\int_{-\infty}^{\infty}\frac{\kappa_0J_0(\kappa_0a)H_1^{(2)}(\kappa_0b)}{Z^a(\alpha)}e^{-j\alpha z}d\alpha. \tag{20}$$

As with (8), (20) can be written as a sum of residues and a branch cut integral

$$I^a(z)=\sum_n I^a_n(z)+I^a_{\rm bc}(z) \tag{21}$$

where

$$I^a_{\rm bc}(z)=\omega\varepsilon_0bk_0\int_0^\infty\frac{ue^{-k_0z\sqrt{u^2-1}}}{\sqrt{u^2-1}}\left[F^{(1)}_-(u)-F^{(2)}_+(u)\right]du$$

with

$$F^{(n)}_\pm(u)=\frac{k_0uJ_0\left(k_0ua\right)H_1^{(n)}\left(k_0ub\right)}{k_0^2u^2J_0\left(k_0ua\right)H_0^{(n)}(k_0ua)\pm 4\omega\varepsilon_0Z_s}. \tag{22}$$

It should be noted that (20) could be obtained in a manner similar to (8), i.e., without the preliminary step of forming an integral equation. However, the integral equation method is worthwhile since it applies to a finite-length wire upon replacing the integration limits $(-\infty,\infty)$ in (16) by $(-h,h)$, where $2h$ is the wire length. For the finite length wire one can not use Fourier transforms to solve the SI-IE, although discretization methods such as the method of moments [31] are widely used, as discussed next.

2) Approximate Solution of the Surface Impedance Integral Equation for a Finite-Length Dipole: In addition to the exact modal solution (9), and the exact solution to the approximate SI-IE (21), a MoM solution of the SI-IE for a finite-length dipole has also been implemented. The numerical solution utilized here

$$F^{(n)}(u)=\frac{J_1(\xi_ma)H_1^{(n)}(k_0ub)}{\varepsilon_mk_0uJ_1(\xi_ma)H_0^{(n)}\left(k_0ua\right)-\varepsilon_0\xi_mJ_0(\xi_ma)H_1^{(n)}(k_0ua)} \tag{12}$$

involves transforming the Pocklington equation (16) (with integration limits $(-h, h)$ for a finite-length dipole) to the Hallén form [32]–[34], resulting in

$$\int_{-h}^{h} \left(K(z-z') + q\left(z-z'\right)\right) I^a(z')dz' = c_1 \sin k_0 z + c_2 \cos k_0 z - \frac{j4\pi}{\eta}\int_0^z E^i\left(z'\right)\sin\left(k_0(z-z')\right)dz' \quad (23)$$

where

$$q(z-z') = 2\pi\omega\varepsilon_0 Z_s \frac{e^{-jk_0|z-z'|}}{k_0}. \quad (24)$$

For the magnetic frill source [33]

$$E^i(z) = \frac{1}{2\ln\left(\frac{b}{a}\right)}\left(\frac{e^{-jk_0\sqrt{a^2+z^2}}}{\sqrt{a^2+z^2}} - \frac{e^{-jk_0\sqrt{b^2+z^2}}}{\sqrt{b^2+z^2}}\right). \quad (25)$$

A rectangular pulse function expansion, point testing solution of (23) was obtained, where matrix entries were computed with the aide of the integrals given in [35].

C. Verification of Solutions

For the infinite dipole, the exact solution of the exact modal (9) and the exact solution of the approximate SI-IE (21) were verified by comparing results with those in [36], which concerns a solid cylindrical infinite-length metallic antenna having finite conductivity. For example, for $f = 300$ MHz, $a = 0.01$ cm, and $\sigma = 8.44 \times 10^4$ S/m, at a position $z = 2$ m from the source the current in [36] was given as $|I| \simeq 420$ μA. Both (9) and (21) yielded $|I| = 427.53$ μA, using the principle pole (i.e., using one residue plus the branch cut integral). The small difference between the results of [36] and the two formulations presented here is probably due to the fact that in [36] a slightly different magnetic-frill source was used (one that presented an annulus of current, rather then an infinitely-thin ring of current). The approximate MoM solution of the SI-IE (23) was verified by comparing to theoretical and experimental results in the literature for perfectly conducting [32], [33] and lossy [8]–[12] finite-length dipoles. In addition, for near-infrared and optical frequencies copper dipole antennas are quite lossy, and can be made sufficiently long so that current diminishes to negligible values before reaching the ends of the wire. In this case the solution of the SI-IE for the infinite length wire, (21), and MoM solution of (23) for the finite-length wire should agree, since they are both solutions to the Pocklington equation. Indeed, for sufficiently long antenna half-lengths h excellent agreement between (21) and the solution of (23) was found. This can be considered to be a good check on the MoM solution of (23), since (21) is obtained simply as an integral and residue, without any (formal) discretization.

III. Results

A. Applicability of the Surface Impedance Integral Equation

A major distinction between the exact modal and approximate SI-IE formulations, (9) and (21), respectively, is the difference between the transcendental eigenvalue equation associated with each method; $Z^e(\alpha) = 0$ for the exact modal method and $Z^a(\alpha) = 0$ for the approximate SI-IE method. For both methods

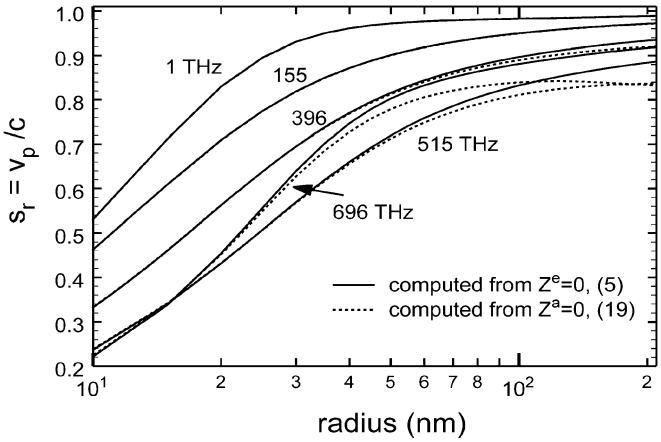

Fig. 1. Normalized phase velocity $s_r = v_p/c$ of the principle mode on an infinite copper wire as a function of radius for several frequencies in the near-infrared and optical regimes. The exact mode (β^e from (5)—solid lines) and the approximate mode (β^a from (19)—dashed lines) are compared.

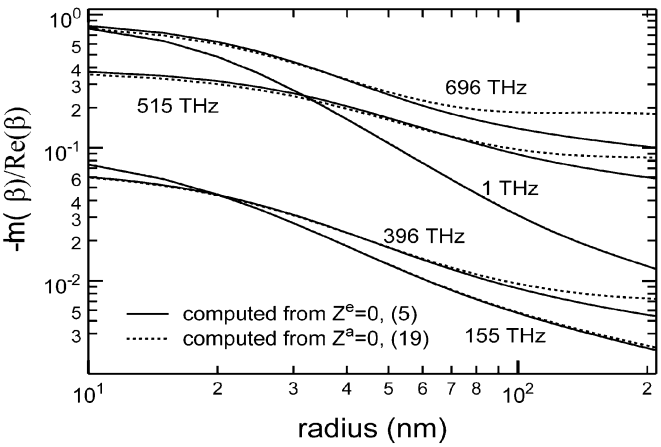

Fig. 2. Relative attenuation, $-\mathrm{Im}(\beta)/\mathrm{Re}(\beta)$, of the principle mode on an infinite copper wire as a function of radius for several frequencies in the near-infrared and optical regimes. The exact mode (β^e from (5)—solid lines) and the approximate mode (β^a from (19)—dashed lines) are compared.

the principle mode is of fundamental importance, and the corresponding wave numbers are denoted by β^e and β^a, respectively.

In order to compare the principle modes of the two methods, Figs. 1 and 2 show results from a root search for the principle mode (performed using standard Newton methods). Fig. 1 shows the normalized phase velocity

$$s_r = \frac{k_0}{\mathrm{Re}(\beta)} = \frac{\omega}{c\mathrm{Re}(\beta)} = \frac{v_p}{c} \quad (26)$$

of the principle mode as a function of the wire radius a at several frequencies in the near-infrared and optical regime for a copper wire ($f = 1$ THz is also shown for comparison). In (26), c is the speed of light in vacuum, and $\beta = \beta^e$ or $\beta = \beta^a$. In Fig. 2 the relative attenuation factor, $-\mathrm{Im}(\beta)/\mathrm{Re}(\beta)$, is shown.

Results are computed using the optical permittivity values for copper listed in [37], from which the conductivity can be computed as

$$\sigma = j\omega\varepsilon_0\left(\frac{\varepsilon}{\varepsilon_0} - 1\right). \quad (27)$$

Values used in this work are collected in Table I for convenience.

TABLE I
MATERIAL PROPERTIES OF COPPER AT SEVERAL FREQUENCIES IN THE NEAR INFRARED AND OPTICAL REGIME. PERMITTIVITY VALUES ARE FROM [37] (WITH THE EXCEPTION OF THE FAR INFRARED $f = 1$ THZ VALUE THAT COMES FROM THE DRUDE MODEL AND IS USED AS A CONTRAST TO THE NEAR IR AND OPTICAL RESULTS), AND CONDUCTIVITY IS COMPUTED FROM (27). THE LAST COLUMN IS RELEVANT TO CLASSIFYING THE MATERIAL AS A GOOD CONDUCTOR (WHEN $|\sigma/\omega\varepsilon| \gg 1$); A DISCUSSION OF THIS ASPECT IS PROVIDED IN THE APPENDIX. $\sigma_0 = 5.9 \times 10^7$ S/M IS THE DC CONDUCTIVITY OF COPPER

f (THz)	$\sqrt{\varepsilon/\varepsilon_0}$	$\lvert\sigma/\sigma_0\rvert$	$\lvert\sigma/\omega\varepsilon_0\rvert$
1	$665.42 - j776.65$	0.986	1.05×10^6
155	$1.09 - j13.43$	0.0267	182.77
396	$0.24 - j4.665$	0.0085	22.77
515	$0.7 - j2.704$	0.0042	8.65
696	$1.25 - j2.305$	0.0049	7.47

From Figs. 1 and 2, two conclusions can be drawn. First, as would be expected, at very small radius values the wave is quite slow, and highly attenuated. This can be explained by simply appealing to the formula for ac resistance of a wire, which shows that $R_{ac} \propto 1/a$ [38]. Second, and of more relevance for this work, the propagation constant from the exact modal formulation and the approximate SI-IE formulation agree very well at small radius values, but the curves begin to separate as the wire radius increases. The point of separation depends on the frequency and associated conductivity. In the upper near-infrared and lower optical range the results agree up to radius values of approximately 50–60 nm, but in the middle and upper optical range the results only agree for radius values less than 30–40 nm. Since the principle mode plays an important (and often dominant) role in determining the wire's current, it might be inferred that the surface impedance integral equation should yield acceptable results for frequencies and radius values where $\beta^a \simeq \beta^e$. The investigation described here generally confirms this suggestion when the principle mode dominants the response, as discussed in more detail below.

Fig. 3 shows the magnitude of the current induced on an infinite copper wire by the magnetic frill source computed using the exact modal formulation (9) (solid lines), and approximate SI-IE formulation (21) (dashed lines). The current is evaluated at $z = 1500$ nm, which is $0.78\lambda_0$ at $f = 155$ THz, $1.98\lambda_0$ at $f = 396$ THz, $2.58\lambda_0$ at $f = 515$ THz, and $3.48\lambda_0$ at $f = 696$ THz. Also shown are the SI-IE MoM results from solving (23) for a finite length, though very long antenna (the wire half-lengths ranged from 6 000 to 60 000 nm, depending on the radius and frequency, to reduce currents to negligible values on the wire ends and therefore simulate an infinite-length dipole). The MoM results are shown as circles in Fig. 3, and it can be seen that excellent agreement between (21) and (23) is obtained (as noted previously, this should be the case since they are both solutions to the Pocklington equation).

From Fig. 3 one can see that agreement between the two methods is very good when $\beta^a \simeq \beta^e$ (shown in Figs. 1 and 2) at the lower frequencies, and is fairly good when $\beta^a \simeq \beta^e$ at higher frequencies. The approximate surface impedance formulation (21) loses accuracy at larger radius values, and higher frequencies. Although the results refer to the location $z = 1500$ nm on an infinite copper wire, these results are fairly representative and the conclusions drawn from the figure are not specific to this

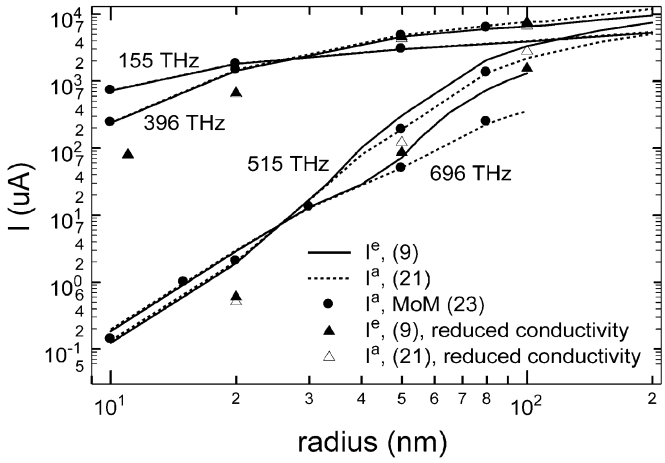

Fig. 3. Magnitude of the current induced on a copper wire by a magnetic frill source, computed using the exact (9) (solid lines) and approximate (21) (dashed lines) formulations. The current is evaluated at $z = 1500$ nm, which is approximately 1–2 wavelengths from the source at the indicated frequencies. In addition, circles indicate the MoM solution for a long, finite-length dipole computed from (23), and solid and hollow triangles indicate results from (21) and (9), respectively, using a reduced conductivity as described later in the text.

TABLE II
PERCENTAGE DIFFERENCE BETWEEN THE EXACT (9) AND APPROXIMATE (21) CURRENT FOR SEVERAL DIFFERENT FREQUENCIES AND RADIUS VALUES ON AN INFINITE COPPER DIPOLE. THE FIRST AND SECOND NUMBERS IN THE PAIR (p_1, p_2) ARE THE PERCENT DIFFERENCES AT DISTANCES OF $z = \lambda$ AND $z = 2\lambda$, RESPECTIVELY, FROM THE SOURCE

a (nm)	$\%\Delta$, 155 THz	$\%\Delta$, 396 THz	$\%\Delta$, 515 THz	$\%\Delta$, 696 THz
10	(0.5, 0.5)	(3, 1)	(10, 10)	(7, 7)
20	(0.5, 0.4)	(4, 3)	(7, 8)	(2, 3)
30	(0.6, 0.5)	(5, 4)	(11, 22)	(14, 14)
50	(0.8, 0.8)	(7, 6)	(3, 30)	(16, 35)
80	(1.2, 1.2)	(10, 9)	(2, 22)	(18, 41)
100	(1.4, 1.4)	(12, 11)	(4, 20)	(18, 45)
150	(2.1, 2.1)	(16, 16)	(7, 18)	(64, 77)
200	(2.7, 2.8)	(19, 20)	(15, 25)	(19, 82)

location. For example, for $a = 50$ nm at 155 THz, for locations ranging from 0 to 3000 nm from the antenna center, the percent differences between the exact modal solution (9) and the exact solution of the SI-IE (21) vary between 0.82% and 1.26%. At 396 THz, the percentage differences vary between 3% and 6%. For higher frequencies the agreement between the two formulations is not as good, and the percentage differences vary more significantly with location, as would be expected.

In order to specify the difference in results more precisely, Table II shows the percent differences $\%\Delta$ between the current calculated using the exact (9) and approximate (21) methods at a distance of one- and two-wavelengths from the source (the first and second numbers in the brackets are the percent differences at the distance $z = \lambda$ and $z = 2\lambda$, respectively). It can be seen that in the near-infrared, at $f = 155$ THz, the agreement is very good for all radius values. At 396 THz the agreement is reasonably good (less than 5% difference) for a approximately 30 nm or less, whereas at 515 and 696 THz agreement between the methods is not generally very good.

As discussed in the Appendix, the surface impedance (14) should be valid when $|\sigma/\omega\varepsilon_0| \gg 1$, which occurs in the IR band

TABLE III
EFFECT OF PRINCIPAL MODE DOMINANCE ON THE ACCURACY OF THE IMPEDANCE BOUNDARY CONDITION FOR A VERY THIN WIRE $a = 10\text{nm}$. z IS DISTANCE FROM THE SOURCE, THE FIRST NUMBER IS THE PERCENTAGE DIFFERENCE BETWEEN THE EXACT (9) AND APPROXIMATE (21) CURRENT ON AN INFINITE COPPER DIPOLE, AND THE NUMBER IN BRACKETS IS THE RATIO OF PRINCIPLE MODE RESIDUE I^e_{res}, AND BRANCH CUT CONTRIBUTION I^e_{bc}

f (THz)	$\%\Delta$, $(\lvert I^e_{res}/I^e_{bc}\rvert)$			
	$z/\lambda = 0.1$	$z/\lambda = 1$	$z/\lambda = 2$	$z/\lambda = 4$
155	0.6, (17)	0.5, (185)	0.4, (243)	0.4, (124)
396	5, (24)	3, (350)	1, (433)	5, (185)
515	8, (18)	10, (10^{-4})	10, (10^{-4})	9, (10^{-11})
696	4, (7)	7, (10^{-3})	7, (10^{-8})	7, (10^{-19})

and at the lower optical frequencies. At higher frequencies this inequality is not satisfied as strongly, and so generally the SI-IE method is not accurate in the middle and upper optical frequencies. However, as seen in Fig. 3 and Table II, the wire radius also plays a significant role, especially for somewhat higher frequencies. For example, when β^e and β^a differ appreciably, such as for larger radius wires (see Figs. 1 and 2), one would anticipate that the SI-IE would be inaccurate since the residue contributions will differ substantially. This is indeed found to be true, and in this case the surface impedance (14) is neither accurate for determining the principle modes on an infinite wire, nor for determining the induced current from the SI-IE. Error percentages between the exact and approximate methods for the current are larger than percent differences in the β values due to the exponential dependence of the current on $\text{Im}(\beta)$.

However, problems also arise for wires of very small radius, where from Figs. 1 and 2 it can be seen that $\beta^e \simeq \beta^a$ even at the upper optical frequencies. The good agreement between the principle modes at the upper optical frequencies can be understood by considering that for extremely small radius values (in the limit as radius goes to zero) the inequality $|\sigma/\omega\varepsilon_0| \gg 1$ is not directly relevant in forming the surface impedance approximation (i.e., in approximating (31) by (33) in the Appendix). However, the surface impedance approximation assumes that the principle mode should be dominant over the branch cut contribution, and this relationship becomes sensitive to the distance from the source at higher frequencies. This is shown in Table III, where a copper wire of radius $a = 10$ nm is considered. The first entry in each column is the percent difference between the exact (9) and approximate (21) current at the indicated distance from the source. The second entry in each column, in brackets, is the ratio of the residue to branch cut contribution at that distance. One can see that, for this extremely small radius wire, at higher frequencies the branch cut contribution tends to dominate the response since the principle mode is strongly damped (see Fig. 2). Thus, for an extremely small radius wire the impedance boundary condition can be used to determine the principle modes on an infinite wire even at upper optical frequencies, yet the SI-IE formulation will not generally lead to an accurate determination of the current except for locations where the principle mode contribution is dominant. This explains why in Table II, for 515 and 696 THz, the percent errors decrease in going from $a = 10$ nm to $a = 20$ nm, since in the latter case the principle mode is dominant at $z = \lambda, 2\lambda$, whereas in the former case it is not. Then, starting at $a = 30$ nm the percent errors start to increase even though the principle mode is dominant, since the error in β^a increases (as seen in Figs. 1 and 2). For 155 and 396 THz this effect is not seen in Table II, since the principle mode is dominant at $z = \lambda, 2\lambda$ even for $a = 10$ nm.

In summary, the SI-IE seems to lead to good accuracy in the IR band, and at lower optical frequencies. In the latter case, if one considers 5% to be an acceptable error, then for $f = 396$ THz, radius values should be less than 50 nm. For the middle and upper optical frequencies the approximate SI-IE method generally is not valid, even when the surface impedance approximation leads to an accurate determination of the principle mode propagation constant (such as for extremely small radius wires). For initial design and analysis, an error percentage of 5% may be considered acceptable and, hence, one may use the approximate IE for the indicated radii and frequencies. An advantage of the approximate IE compared to e.g., volume integral equations is its relative simplicity.

B. Reduced Conductivity

One other set of data is shown in Fig. 3, labeled "reduced conductivity," and given by solid or hollow triangles. These results are from the exact modal solution (9) and exact solution of the SI-IE (21) using values of conductivity that are less then the bulk values provided in [37]. It is somewhat obvious that lower than bulk values of conductivity may be important to consider, since as the dimensions of a material shrink to the nanoscale the properties of the material will change. This change is due to several factors, such as the increased importance of surface effects as the surface to volume ratio of nanostructures becomes large. Also, when the dimensions of the structure approach the Fermi wavelength of electrons, quantum confinement effects must be accounted for. Fortunately, it has been shown that quantum confinement effects only need to be accounted for in metallic structures much smaller than 10 nm [39], [40], due to the Fermi wavelength in metals being sub 1 nm. Therefore, in general, the macroscopic model of Maxwell's equations together with an appropriate material dispersion equation is valid for metals having dimensions on the order of 5–10 nm or more. However, non-quantum size effects are generally present for metals having dimensions on the order of, or smaller, than the electronic mean free path [40], which is approximately 40 nm for copper. These size effects include both grain boundary scattering, and increased surface scattering.

At this time the value of dc conductivity for circular cross-section metal cylinders having radius values on the order of the mean free path, or less, can only be estimated. For example, recent measurements on rectangular cross-section copper traces indicate that when transverse dimensions fall below 100 nm, surface and grain boundary scattering cause a significant increase in dc resistivity. In particular, for the 50 nm $\times$ 50 nm copper traces considered in [41], the measured dc resistivity was approximately twice as large as the bulk value for copper. Using an effective radius of $a = 23$ nm (which results in a cylinder that has the same cross-sectional area as in the rectangular case), we can estimate that for this small radius the value of conductivity should be perhaps halved from the bulk

value. However, note that in [41] it is indicated that a significant amount of impurities are present in the samples, and, further, that strong grain boundary scattering occurs, which is dependent on fabrication methods. Also, one would expect more significant scattering from rectangular cross-section structures than for circular cross-section structures, and so the estimates obtained from [41] are probably worst case dc values (and ac σ values may tend to be less influenced by size-dependent effects). However, this observation does not mean that the effect of lower conductivity on the antenna performance of circular cross-section structures is not worthwhile to consider. So, in Fig. 3 the symbols labeled "reduced conductivity" indicate results from (9) and (21) for $f = 396$ THz and $f = 515$ THz where a diminished conductivity is used. Taking estimates from [41], at $a = 10$ nm and $a = 20$ nm the conductivity was multiplied by 0.58, at $a = 50$ nm, conductivity was multiplied by 0.80, and for $a = 100$ nm, conductivity was multiplied by 0.88. Although the current magnitude was affected significantly, at $f = 396$ THz the results from (9) and (21) are indistinguishable on the scale of the plot until fairly large radius values, which verifies the surface impedance boundary condition method even for this lower conductivity. For $f = 515$ THz the difference is noticeable at smaller radius values, in line with the results that were obtained using the bulk values [solid triangles are the results from the approximate formulation (21), and hollow triangles are the results from the exact formulation (9)].

Therefore, we can conclude that in the near-infrared region the approximate SI-IE formulation yields results that agree well with the exact modal method (for the range of radius values considered here), for the lower optical frequencies the approximate SI-IE method is adequate for sufficiently small radius wires (approximately under 50 nm), and for the middle to upper optical frequencies the surface impedance boundary condition formulation does not generally lead to an accurate formulation.

IV. Discussion of Optically Resonant Dipoles

It should be kept in mind that although radius values in the considered range may seem quite small, in the near-infrared and optical range the dipole half-lengths at first resonance are approximately $h \simeq s_r \lambda_0/4$, where, from Fig. 1 it can be seen that the s_r values can be quite small for nanoscale radius wires. For example, from Fig. 1 at $f = 396$ THz for $a = 50$ nm, $s_r \simeq 0.815$, and so the half-length of the resonant dipole would be $h \simeq 154$ nm. Based on the MoM solution to (23), the actual resonate half-length was found to be $h \simeq 110$ nm. For these values $2h/a = 4.4$ and $k_0 a = 0.415$, which constitutes a relatively thick dipole by conventional standards (for example, in the megahertz and gigahertz range, one often has $2h/a = 100$–1000, or even larger, and $k_0 a = 0.001$–0.0001, or smaller). A relatively large value of $2h/a$ is necessary to achieve good polarization selectivity, and to insure negligible circumferential currents that can degrade radiation patterns. Although one can tune the resonance by choosing the dipole radius appropriately (thereby adjusting the factor s_r from Fig. 1), when a becomes too small losses on the antenna increase significantly, and when a becomes too large compared to h, polarization selectivity is diminished. Therefore, there is an inherent trade-off between loss (which is usually not a factor at megahertz and gigahertz frequencies) and polarization selectivity (which is an attribute that is taken for granted in the megahertz and gigahertz range since thin wires are typically utilized). In the optical range it is difficult to simultaneously achieve very low loss and large $2h/a$ values for resonant dipoles, since the resonant half-length is small. For example, as a rough guide, the half-length of a resonant dipole is approximately $h = 363$ nm at $f = 155$ THz, $h = 142$ nm at $f = 396$ THz, $h = 109$ nm at $f = 515$ THz, and $h = 81$ nm at $f = 696$ THz, where $s_r = 0.75$ is used as a representative value for comparison purposes. Based on MoM modeling, the actual resonant lengths may be smaller.

TABLE IV
Efficiency and Input Impedance for an $h = 110$ nm Copper Dipole at 396 THz. (a) Using $\sigma_{cu} = 4.93 \times 10^4 - j5.00 \times 10^5$ S/m, (b) Using $\sigma = 0.58\sigma_{cu}$

a (nm)	e_r	Z_{in}
10	0.24	$839.66 - j1152.89$
20	0.62	$92.63 + j149.72$
30	0.77	$51.55 + j37.62$
40	0.84	$43.36 + j10.51$
50	0.87	$40.46 + j0.636$
60	0.90	$39.06 - j3.74$

(a)

a (nm)	e_r	Z_{in}
10	0.04	$133.97 - j210.09$
20	0.47	$394.43 + j491.10$
30	0.68	$81.88 + j126.98$
40	0.79	$54.16 + j55.52$
50	0.85	$45.56 + j29.36$
60	0.89	$41.58 + j16.93$

(b)

In the upper optical frequencies, where resonant half-lengths atre well under 100 nm and conductivity values are relatively low, the concept of an optical thin-wire dipole may not be feasible. In contrast, in the near-infrared and lower optical frequencies resonant dipoles with acceptable efficiencies and polarization selectivities may be obtainable. In Table IV some preliminary results [from (23)] for the efficiency ($e_r = P_r/P_{\text{in}}$, where P_r and P_{in} are the radiated and input power, respectively) and input impedance ($Z_{\text{in}} = 1/I_{\text{in}}$) of a finite-length dipole at 396 THz are provided for several reasonable radius values. The dipole half-length is $h = 110$ nm, such that the antenna is near its first resonance when $a = 50$ nm. In Table IV(a), we show results using the bulk value of conductivity, and in Table IV(b) the bulk value was multiplied by 0.58 to assess the effect of reduced conductivity on efficiency. As expected, for very small radius values the efficiency is quite low. Reasonable efficiencies can be obtained for radius values on the order of 50 nm or larger. Although the conductivity value was reduced by 58% in Table IV(b), the efficiency only changed by 2.3% for $a = 50$ nm. A much larger percent change is found for smaller radius wires.

Since at resonance ($a = 50$ nm) the dipole is not very thin in the sense that $2h/a = 4.4$ is not a large value, and $k_0 a = 0.415$ is not very small, the presence of end caps and circumferential current contributions, which are ignored here, may be important, and should be assessed in future research.

V. Conclusion

The validity of using the common surface impedance integral equation for near-infrared and optical copper dipole antennas has been assessed. To this end, results from an exact modal solution for an infinite cylinder, from an exact solution of the approximate SI-IE for an infinite cylinder, and the approximate MoM solution of the SI-IE for a finite-length cylinder have been compared. It has been found that the SI-IE formulation, which is based on an impedance boundary condition, yields results that should be accurate in the near-infrared, and at the lowest optical frequencies subject to certain restrictions on the wire's radius. For the middle and upper optical frequencies, the approximate SI-IE is generally not valid. For combinations of radius and frequency values where the SI-IE is not appropriate, one must use either a volume IE, or surface equivalence principle based IE, or some other method, such as FDTD, to analyze the antenna. Furthermore, it has been shown that since resonant half-lengths are small in the upper near-infrared and optical range (on the order of 100 nm), it becomes important to acknowledge the trade-off between radiation efficiency (related to the wire's radius) and maintaining a large length-to-radius ratio, which impacts polarization selectivity and radiation patterns. Finally, some representative values for the efficiency and input impedance of a half-wave resonant optical copper dipole have been presented. Further investigation, both experimental and numerical, of the antenna properties of optical and near-infrared dipoles is warranted.

Appendix
Derivation of the Surface Impedance

The surface impedance (14) can be derived starting with an infinite lossy dielectric cylinder, as considered in Section II-A. As described in [42, p. 528], although there is more than one zero of $Z^e(\alpha) = 0$, only the principle zero (sometimes called the Sommerfeld mode) is not severely damped when the cylinder is a relatively good conductor. Denoting this zero by β_0, and the resulting residue current by $I^e_{\beta_0}$, (8) reduces to

$$I^e(z) \simeq I^e_{\beta_0}(z) + I^e_{\rm bc}(z). \tag{28}$$

Assuming that for sufficiently large z $\left|I^e_{\beta_0}(z)\right| \gg |I_{\rm bc}(z)|$, then $I^e(z) \simeq I^e_{\beta_0}$. In this case

$$I^e_{\beta_0}(z) = -2\pi\omega\varepsilon_m\varepsilon_0 b \frac{J_1(\kappa_m a)\, H_1^{(2)}(\kappa_0 b)}{Z^{e\prime}(\beta_0)} e^{-j\beta_0 z} \tag{29}$$

where $Z^{e\prime}(\beta_0) = dZ^e(\alpha)/d\alpha|_{\alpha=\beta_0}$. Defining a surface impedance per unit length Z_s, as

$$Z_s = \frac{E_s(z)}{I^e_{\beta_0}(z)} \tag{30}$$

where E_s is the tangential (axial) electric field evaluated at $\rho = a$, we obtain

$$Z_s = \frac{\kappa_m J_0(\kappa_m a)}{2\pi a j\omega\varepsilon_m J_1(\kappa_m a)}. \tag{31}$$

This form of the surface impedance depends on β_0 via $\kappa_m^2 = k_m^2 - \beta_0^2$, and so it can be used in, for example, the infinite dipole model for the root search of (19), and in the exact solution of the SI-IE, (21) (although the form (14) was used in obtaining numerical results in this work). However, this form is not desirable for the MoM solution of (23) since usually one wants to have an expression for surface impedance that is independent of the propagation constant. To obtain this result one notes that in the limit of infinite conductivity, $\beta_0 = k_0$ [42], and for finite yet sufficiently large conductivity, $\beta_0 \simeq k_0$ (as can be seen from Fig. 1, even for extremely small radius wires β_0 is within an order of magnitude of k_0). Assuming $|\sigma/\omega\varepsilon_0| \gg 1$, where σ is the conductivity of the metal (S/m), then $|k_m| \gg k_0$ and $\kappa_m^2 \simeq k_m^2$. Writing

$$\begin{aligned} k_m &= \omega\sqrt{\mu_0\varepsilon_0\left(1 - \frac{j\sigma}{\omega\varepsilon_0}\right)} \\ &\simeq (1-j)\sqrt{\frac{\omega\mu_0\sigma}{2}} = \gamma \end{aligned} \tag{32}$$

we obtain the well-known expression for surface impedance [approximating $j\omega\varepsilon_m$ by σ, from (27)],

$$Z_s = \frac{\gamma J_0(\gamma a)}{2\pi a\sigma J_1(\gamma a)}. \tag{33}$$

Despite the optical conductivity of copper being quite small compared to the dc value, the ratio $|\sigma/\omega\varepsilon_0|$ is greater then one, as shown in the last column of Table I. Thus, in the optical range the approximation $k_m \simeq \gamma$ is not nearly as good as in the IR band, although it still holds somewhat.

From the results presented here, it is also clear that the surface impedance approximation is generally better at very small radius values. This is because for sufficiently small radius, both (31) and (33) reduce to

$$Z_s = \frac{1}{\pi a^2\sigma} \tag{34}$$

as $\kappa_m a$ and $\gamma a \to 0$. Thus, for very small radius values the relatively poor approximation (at optical frequencies) $k_m \simeq \gamma$ is not relevant, although one still should have the principle mode dominate over the branch cut contribution, which was assumed in forming (31). Physically, in this case the field inside the wire will be approximately constant, and the field value at the wire surface will capture the physics internal to the wire. For larger radius values skin effects will cause the field within the wire to vary significantly as a function of radial distance.

Acknowledgment

The author would like to thank the reviewers for thoughtful comments that significantly improved the text.

References

[1] Z. Liu and Y. Bando, "A novel method for preparing copper nanorods and nanowires," *Adv. Mater*, vol. 15, pp. 303–305, 2003.

[2] P. I. Wang, Y. P. Zhao, G. C. Wang, and T. M. Lu, "Novel growth mechanism of single crystalline Cu nanorods by electron beam irradiation," *Nanotechnology*, vol. 15, pp. 218–222, 2004.

[3] D. W. Pohl, "Near field optics seen as an antenna problem," in *Proc. Near-Field Optics: Principles and Applications, The Second Asia-Pacific Workshop on Near-Field Optics*, Beijing, China, Oct. 1999.
[4] C. Giradr, "Near fields in nanostructures," *Rep. Prog. Phys.*, vol. 68, pp. 1883–1933, 2005.
[5] J. J. Greffet, "Nanoantennas for light emission," *Science*, vol. 308, pp. 1561–1563, 2005.
[6] J. Alda, J. M. Rico-García, J. M. López, and G. Boreman, "Optical antennas for nano-photonic applications," *Nanotechnology*, vol. 16, pp. S230–S234, 2005.
[7] C. Fumeaux, J. Alda, and G. D. Boreman, "Lithographic antennas at visible frequencies," *Opt. Lett.*, vol. 24, pp. 1629–1631, 1999.
[8] T. T. Wu and R. W. P. King, "The cylindrical antenna with nonreflecting resistive loading," *IEEE Trans. Antennas Propag.*, vol. AP-12, pp. 369–373, May 1964.
[9] R. W. P. King and T. T. Wu, "The imperfectly conducting cylindrical transmitting antenna," *IEEE Trans. Antennas Propag.*, vol. AP-14, pp. 524–534, Sep. 1966.
[10] C. D. Taylor, C. W. Harrison, and E. A. Aronson, "Resistive receiving and scattering antenna," *IEEE Trans. Antennas Propag.*, vol. AP-15, pp. 371–376, May 1967.
[11] J. H. Richmond, "Scattering by imperfectly conducting wires," *IEEE Trans. Antennas Propag.*, vol. AP-15, pp. 802–806, Nov. 1967.
[12] B. D. Popović and Z. D. Popović, "Imperfectly conducting cylindrical antenna: Variational approach," *IEEE Trans. Antennas Propag.*, vol. AP-19, pp. 435–536, May 1971.
[13] O. J. F. Martin, C. Girard, and A. Dereux, "Generalized field propagator for electromagnetic scattering and light confinement," *Phys. Rev. Lett.*, vol. 74, pp. 526–529, 1995.
[14] J. C. Weeber, A. Dereux, Ch. Girard, G. C. Des Francs, J. R. Krenn, and J. P. Goudonnet, "Optical addressing at the subwavelength scale," *Phys. Rev. E.*, vol. 62, pp. 7381–7388, 2000.
[15] M. Paulus and O. J. F. Martin, "Light propagation and scattering in stratified media: A Green's tensor approach," *Opt. Soc. Amer. A*, vol. 18, pp. 854–861, 2001.
[16] T. Søndergaard and B. Tromborg, "Lippmann-Schwinger integral equation approach to the emission of radiation by sources located inside finite-sized dielectric cylinders," *Phys. Rev. E*, vol. 66, pp. 155309:1–13, 2002.
[17] V. A. Podolskiy, A. K. Sarychev, E. E. Narimanov, and V. M. Shalaev, "Resonant light interaction with plasmonic nanowire systems," *J. Opt. A*, vol. 7, pp. S32–S37, 2005.
[18] D. P. Fromm, A. Sundaramurthy, P. J. Schuck, G. Kino, and W. E. Moerner, "Gap-dependent optical coupling of single "bowtie" nanoantennas resonant in the visible," *Nano Lett.*, vol. 4, no. 5, pp. 957–961, 2004.
[19] P. J. Schuck, D. P. Fromm, A. Sundaramurthy, G. S. Kino, and W. E. Moerner, "Improving the mismatch between light and nanoscale objects with gold bowtie nanoantennas," *Phys. Rev. Lett.*, vol. 94, pp. 017402:1–4, 2005.
[20] E. N. Grossman, J. A. Koch, C. D. Reintsema, and A. Green, "Lithographic dipole antenna properties at 10 μm wavelength: Comparison of method-of-moments predictions with experiment," *Int. J. Infrared. Millimeter Waves*, vol. 19, pp. 817–824, 1998.
[21] J. N. Farahani, D. W. Pohl, H.-J. Eisler, and B. Hecht, "Single quantum dot coupled to a scanning optical antenna: A tunable superemiter," *Phys. Rev. Lett.*, vol. 95, pp. 017402:1–4, 2005.
[22] H.-J. Mühlschlegal, O. Eisler, J. F. Martin, B. Hecht, and D. W. Pohl, "Resonant optical antennas," *Science*, vol. 308, pp. 1607–1609, 2005.
[23] D. S. Jones, *Methods in Electromagnetic Wave Propagation*. New York: IEEE Press, 1994.
[24] E. Hallén, *Electromagnetic Theory*. New York: Wiley, 1962.
[25] T. T. Wu, "Introduction to linear antennas," in *Antenna Theory*, R. E. Collin and F. J. Zucker, Eds. New York: McGraw-Hill, 1969, ch. 8, pt. 1.
[26] C. M. Butler and D. R. Wilton, "Analysis of various numerical techniques applied to thin-wire scatterers," *IEEE Trans. Antennas Propag.*, vol. 23, pp. 534–540, Jul. 1975.
[27] D. R. Wilton and C. M. Butler, "Efficient numerical techniques for solving Pocklington's equation and their relationships to other methods," *IEEE Trans. Antennas Propag.*, vol. 24, pp. 83–86, Oct. 1976.
[28] D. S. Jones, "Note on the integral equation for a straight wire antenna," *Proc. Inst. Elect. Eng.*, vol. 128, pp. 114–116, Apr. 1981.
[29] A. G. Tijhuis, P. Zhongqiu, and A. M. Bretones, "Transient excitation od a straight thin-wire segment: A new look at an old problem," *IEEE Trans. Antennas Propag.*, vol. 40, pp. 1132–1146, Oct. 1992.
[30] B. P. Rynne, "On the well-posedness of Pocklington's equation for a straight wire antenna and convergence of numerical solutions," *J. Electromagn. Waves Applicat.*, vol. 14, pp. 1489–1503.
[31] R. F. Harrington, *Field Computation by Moment Methods*. New York: Wiley-IEEE Press, 1993.
[32] R. S. Elliott, *Antenna Theory and Design*. New York: Prentice-Hall, 1981.
[33] W. L. Stutzman and G. A. Thiele, *Antenna Theory and Design*, 2nd ed. New York: Wiley, 1998.
[34] G. W. Hanson, "Fundamental transmitting properties of carbon nanotube antennas," *IEEE Trans. Antennas Propag.*, vol. 53, pp. 3426–3435, Nov. 2005.
[35] D. H. Werner, J. A. Huffman, and P. L. Werner, "Techniques for evaluating the uniform current vector potential at the isolated singularity of the cylindrical wire kernel," *IEEE Trans. Antennas Propag.*, vol. 42, pp. 1549–1553, Nov. 1994.
[36] J. H. Richmond, "Admittance of infinitely long cylindrical wire with finite conductivity and magnetic frill excitation," *IEEE Trans. Antennas Propag.*, vol. AP-27, pp. 264–266, Mar. 1979.
[37] P. B. Johnson and R. W. Christy, "Optical constants of the noble metals," *Phys. Rev. B*, vol. 6, pp. 4370–4379, July 1972.
[38] M. A. Plonus, *Applied Electromagnetics*. New York: McGraw-Hill, 1978.
[39] J.-Y. Bigot, V. Halté, J. C. Merle, and A. Daunois, "Electron dynamics in metallic nanoparticles," *Chem. Phys.*, vol. 251, pp. 181–203, 2000.
[40] C. F. Bohren and D. R. Huffmann, *Absorption and Scattering of Light by Small Particles*. New York: Wiley, 1983.
[41] W. Steinhögl, G. Schindler, G. Steinlesberger, M. Traving, and M. Engelhardt, "Comprehensive study of the resistivity of copper wires with lateral dimensions of 100 nm and smaller," *J. Appl. Phys.*, vol. 97, pp. 023706:1–7, 2005.
[42] J. A. Stratton, *Electromagnetic Theory*. New York: McGraw-Hill, 1941.

George W. Hanson (S'85–M'91–SM'98) was born in Glen Ridge, NJ, in 1963. He received the B.S.E.E. degree from Lehigh University, Bethlehem, PA, the M.S.E.E. degree from Southern Methodist University, Dallas, TX, and the Ph.D. degree from Michigan State University, East Lansing, in 1986, 1988, and 1991, respectively.

From 1986 to 1988, he was a Development Engineer with General Dynamics, Fort Worth, TX, where he worked on radar simulators. From 1988 to 1991, he was a Research and Teaching Assistant in the Department of Electrical Engineering, Michigan State University. He is currently an Associate Professor of electrical engineering and computer science at the University of Wisconsin, Milwaukee. His research interests include nanoelectromagnetics, mathematical methods in electromagnetics, electromagnetic wave phenomena in layered media, integrated transmission lines, waveguides, and antennas, and leaky wave phenomena.

Dr. Hanson a Member of the International Scientific Radio Union (URSI) Commission B, Sigma Xi, and Eta Kappa Nu. He is an Associate Editor for the IEEE TRANSACTIONS ON ANTENNAS AND PROPAGATION.